MMA Memo: 225:
Radiometer Calibration at the Cassegrain Secondary Mirror

Douglas Bock, Jack Welch, Matt Fleming, and Doug Thornton
Radio Astronomy Laboratory
University of California
Berkeley, CA 94720

1. Introduction

Accurate radiometer calibration for millimeter wave telescopes is an important goal. Well calibrated observations better permit the inference of physical properties of the observed sources. In particular, meaningful comparisons of observations taken at different wavelengths or with different instruments depend on accurate calibrations of the various instruments.

The technique presently used at most millimeter telescopes is the "Chopper Wheel Method" introduced by Penzias and Burrus (ARAA, 1973, 11,51), in which the output deflection of an observed source is compared with the difference between the sky brightness and that of an ambient temperature load. The physical temperature of the absorbing atmosphere is then taken to be the same as the ambient load or a mean model of the atmosphere is used. The method is convenient to use, and absolute accuracies of a few percent are typically obtained. Obtaining accuracies at the level of 1% or better requires the use of two black-body loads.

We describe here a scheme in which the calibration loads are introduced in sequence at the center of the secondary mirror of a symmetric Cassegrain telescope. The loads are coupled through a small hole in the center of the secondary which has a diameter equivalent to the aperture blockage of the secondary with respect to the primary. The two loads have temperatures of 300K and 400K, respectively, and are alternately presented to the Cassegrain focus feed by a 45^o flat mirror behind the secondary hole. After calibration has been accomplished, the 45^o mirror is rotated to a third position which presents a concave conical mirror to scatter ambient radiation from the vertex window away from the feed. The coupling to the feed horn will be $1-2\%$, providing a difference signal of 1-2K to the radiometer on top of the antenna temperature. Because the fluctuating brightness of the atmosphere will be present during the calibration, the 45^o mirror may be spun rapidly for a rapid comparison between the loads.

In the following sections we describe the various components of the calibration system and conclude with a discussion of expected errors. We also describe a procedure for measuring the atmospheric extinction.

2. Coupling hole in the Secondary Mirror

Figure 1 shows the Cassegrain optics with a ray leading from the edge of the vertex window to the feed after reflection from the secondary. The locus of other rays that couple the vertex window to the feed reflect from the secondary closer to the optical axis and are usually scattered to the outer parts of the primary by the cone showed as a dotted line. We use the part of the secondary that is normally covered by the cone as the coupling hole for the calibration loads. We assume that when the 45^o mirror images one of the loads in the hole that the hole has a uniform brightness at that temperature. The radius of the hole is b and that of the secondary is R_o. If g(r) is the axially symmetric feed horn gain projected onto the secondary, then the coupling of the small aperture to the feed, k, is given by:

$$k = \frac{\int_0^b g(r) r dr}{\int_0^{R_o} g(r) r dr} \tag{1}$$

This expression ignores the spillover past the secondary which is typically $5 - 10\%$. A simple approximation to the feed pattern is given by

$$g(r) = g_0 (1 - a(r/R_o)^2)^2 \tag{2}$$

which gives the following for the coupling.

$$k = \frac{b^2 3a}{R_o^2 (1 - (1-a)^3)} \tag{3}$$

For the BIMA 6.1m antennas, the secondary mirror diameter is 60.96 cm and the coupling hole diameter is 5.84cm. The illumination at the edge of the secondary is about -10 db (i.e., a = 0.68). Thus the we find k=.0195, or about 2%.

3. The Black Body Loads

Figure 3 shows one of the loads, a simple metal cone with absorbing material glued to its inner surface. The conical shape insures high emissivity. Relative to the normal to the cone base, the slope of the inner surface is at an angle close to the Brewster angle, so that an incident ray with its polarization normal to the surface would be absorbed upon reflection. The other polarization would be absorbed after many scatterings before reaching the vertex. Castable Eccosorb from Emerson & Cumming would be a good candidate for the absorbing material. Note that because the conical load is such a good match, its brightness is not critically dependent on its orientation.

The metal cone will be embedded in insulating material which is transparent to the millimeter/submillimeter waves emitted by the load. The metal part of the conical load will have its temperature regulated to an accuracy and stability of .01K (RMS). This expected accuracy is based on our experience with regulating the temperature of the electronics on our present front ends. The temperature will be sensed by an array of thermistors, and the metal will be heated by a wraparound heater. The servo control will be analog, using a circuit already developed for control of the receiver electronic components. Emerson & Cumming have an insulator, Eccosorb Q, made of fused quartz fibers which has two important features for this application. First, the fused quartz is transparent to millimeter/submillimeter wavelengths. Second, it can withstand very high temperatures, easily higher than the 400K planned for one of the two loads, which many insulators cannot. For the 2% coupling for the BIMA antennas discussed above, the difference between the two loads at temperatures of 300K and 400K will provide a calibrate signal of ΔT_{cal}=2K. Note that we expect the temperature regulation of the metal parts of the loads to be stable to .01K. The ambient temperature of the space where the loads will be located will vary over a large range, on the order of 50K. This variation will produce a small variation in the radiating surface temperature of the load, and, as a result, the effective black body temperature will be stable only to 0.1K. Nevertheless, the ΔT_{cal} should be stable to .002K, that is, to a fractional accuracy of 10^{-3}.

4. Load Mechanical Arrangement

Figure 4 shows two views of the neighborhood of the secondary mirror. One is a side view, and the other is an axial view. The 45^o mirror can rotate about the axis of the telescope. Depending on its angle of rotation, it brings an image of either of the two loads or a scattering mirror (to be discussed below) to the hole in the secondary. The 45^o mirror will be rotated by a stepping motor and can be stopped at each load or the scattering mirror. It can also rotate continuously for a rapid comparison between the loads. For example, 600 RPM corresponds to a 10 Hz chop. Because the fluctuating brightness of the atmosphere is present during this calibration, it will be usually necessary to make a rapid comparison between the loads.

The scattering mirror, which can be imaged in the secondary mirror hole, takes the place of the scattering cone discussed above. This mirror is conical and concave with a cone angle of 4.3^o for the BIMA optics. Figure 2 shows how rays leaving the Cassegrain feed fall on the the primary mirror outside the vertex window after being reflected from the conical mirror. As rays below the axial line are reflected above the line toward the primary, there is no vignetting by the hole in the secondary. The scheme works with sufficient margin that it is also effective for the off axis feeds.

5. Sensitivity Considerations

The calibration signal will be approximately 2K at all wavelengths. It's precise value will be determined by occasional comparison with large sized loads which can be placed over the vertex window. One could be at ambient temperature and the other at, say, liquid nitrogen temperature.

With care, this primary calibration can be made to an accuracy of a few tenths of a percent. As a result, the secondary calibration loads should provide that level of precision.

Consider the following expected system numbers for the MMA: BW = 8 GHz, and Tsys(300GHz) = 50K. In a one second measurement, σ_T=.0006K. In that time the calibration signal is measured with S/N =4000, more than adequate for continuum measurements. In a ten second measurement, a one MHz spectral channel can be calibrated to an accuracy of 1%. Thus this calibration scheme should be useful for spectral bandpass calibration, as well as wide band calibration.

6. Correction for Extinction

Unlike the Chopper Wheel method which provides a calibration with atmospheric extinction automatically taken into account, the present plan requires a separate observation of the extinction by means of tipping curves. The secondary mirror calibration fixes the radiometer scale. The output due to an input power T_{in} is

$$O = K_c T_{in} + O_o \tag{4}$$

with

$$k_c = \frac{\Delta O_{cal}}{\Delta T_{cal}} \tag{5}$$

and O_o, the zero point, is determined by simply turning off the input amplifiers.

The input to the receiver has several components.

$$T_{in}(z) = T_0\alpha(z) + T_{RCVR} + T_{BB}e^{-\tau_o secz} + < T_{air} > (1 - e^{-\tau_o secz}) \tag{6}$$

$T_0\alpha(z)$ is the bare antenna temperature with no atmosphere or background radio sources. It will have a small zenith angle dependence due to variable ground pickup. It must be separately calibrated by means of numerous tipping curves which allow the other components, including the time variable atmospheric emission, to be removed. It should be constant, except for the scaling to the current ambient temperature, for zenith angles less than about 60^o. At longer zenith angles, the antennas will begin to see each other in the spillover, especially in the more compact arrays. T_{RCVR} is the receiver noise temperature. T_{BB} is the effective temperature of the 2.74K background. The last term is the contribution of the atmosphere with the assumption that the air temperature is constant with altitude. A more comprehensive model could be used but probably is unnecessary. With small optical depth, the last term is approximately $< T_{air} > \tau_o secz$.

Tipping curves, measuring $T_{in}(z)$, should be made with a large number of antennas in the array to produce an accurate average curve, one in which the atmospheric brightness fluctuations are averaged out. The range of z should be to z=60^o from the zenith. With $T_0\alpha(z)$ known, T_{RCVR} can be found from the intercept on the secz=0 axis along with the factor $< T_{air} > \tau_o$ by the least squares fitting of the equation. The goal is to find τ_o so that the measured visibilities and antenna temperatures can be corrected by the factor $e^{\tau_o secz}$.

7. Discussion of Errors

The sensitivity discussion above suggests that the basic receiver calibration should be accurate to about 10^{-3}. We now consider the probable errors resulting from the extinction correction. The sensitivity in the atmospheric emission term is more evident if we use the approximate form:

$$< T_{air} > (1 - e^{-\tau_o secz}) \approx < T_{air} > \tau_o secz \tag{7}$$

The fit of the tipping curve is with respect to the variable secz. The term T_{BB} is small, and $T_{BB}$is known. Either an average value of τ_o may be used for this term, or it may be found by iteration in the fit. Suppose the fitting uncertainty in the factor $< T_{air} > \tau_o$ is ϵ. Then

$$\Delta(< T_{air} > \tau_o) = \epsilon = \delta < T_{air} > \tau_o + < T_{air} > \delta\tau_o \tag{8}$$

Since the errors are uncorrelated,

$$\delta\tau_o = \frac{\epsilon + \delta < T_{air} > \tau_o}{< T_{air} >} \tag{9}$$

Representative values for the uncertainties are: ϵ=0.5K for the fitting, $\delta < T_{air} > \approx$ 10K, $< T_{air} > \approx$ 280K and τ_o 0.2, which lead to $\delta\tau_o = .009$. For z=60^o, the correction error is

$$e^{\delta\tau_o secz} = 1.018 \tag{10}$$

This is an error of about 2%.

It is instructive to work out the corresponding errors in the use of the "Chopper Wheel" calibration. In the observation of a radio source which yields an antenna temperature T_s, we make three measurements. O_1 is the output from an observation of the sky near the source.

$$O_1 = k[T_0\alpha(z) + T_{RCVR} + T_{BB}e^{-\tau_o secz} + < T_{air} > (1 - e^{-\tau_o secz})] \tag{11}$$

O_2 is the output with an ambient load in front of the vertex window.

$$O_2 = k[T_0 + T_{RCVR}] \tag{12}$$

O_3 is the output with the antenna pointed at the source.

$$O_3 = k[T_0\alpha(z) + T_{RCVR} + T_{BB}e^{-\tau_o secz} + < T_{air} > (1 - e^{-\tau_o secz}) + T_s e^{-\tau_o secz}] \tag{13}$$

Then

$$O_3 - O_1 = kT_s e^{-\tau_o secz} \tag{14}$$

We can find k from $O_2 - O_1$.

$$O_2 - O_1 = k[T_0 - T_0\alpha(z) - T_{BB}e^{-\tau_o secz} - < T_{air} > (1 - e^{-\tau_o secz})] \tag{15}$$

Finally, the source antenna temperature, T_s, is given by

$$T_s = [O_3 - O_1]\frac{e^{\tau_o secz}}{k} = \tag{16}$$

$$\frac{(O_3 - O_1)[(T_0 - T_0\alpha(z) - < T_{air} >)e^{\tau_o secz} - T_{BB} + < T_{air} >]}{(O_2 - O_1)} \tag{17}$$

The important point is that the main term in the right hand braces is $< T_{air} >$, which does not depend on the extinction. In addition, it is usually assumed that T_0 and $< T_{air} >$ are approximately the same and equal to about 280K, a mean air temperature. The other terms in the right hand braces are indeed small, but they are also not well known, at least in part because the extinction is not known. Altogether, the unknown quantities are $T_0\alpha(z)$, T_0, $< T_{air} >$, and $\tau_o secz$. An estimate of the fractional error in using equation (17) , $\Delta T_s/T_s$, is:

$$\frac{e^{\tau}(\delta T_0\alpha(z) + \delta T_0) + (e^{\tau} - 1)\delta < T_{air} > + [T_0(1 - \alpha(z)) - < T_{air} >]e^{\tau}\delta\tau}{< T_{air} >}, \tag{18}$$

where $\tau = \tau_o secz$. For the various terms we estimate the following values which are consistent with the errors used in the calculation above for the calibration scheme proposed in this memo. $\tau_o secz$=0.4, $\delta T_0\alpha(z)$=5K, $\delta < T_{air} >$=10K, δT_0=10K, $< T_{air} > \approx$ 280K, $\delta\tau_o secz$=0.4, and $(T_0 - T_0\alpha(z) - < T_{air} >) \approx$ 15K. The final error is 9.5%. This is about 5 times larger than the other estimate above. Some of these parameters could be measured, which would improve the accuracy. At the same time, a measurement of the air temperature for the scheme proposed in this memo could reduce its uncertainty significantly. It seems that the greater error for the "chopper wheel" method is inherent in the lack of having two loads to establish the temperature scale independent of using a model for the atmosphere. The penalty is the need to make the tipping curves. However, that measurement should only take a few minutes, and the improved accuracy is probably worth the effort.

8. Conclusions

The proposed plan, in which we have two black body loads weakly coupled at the secondary mirror has a number of advantages.

- Calibration accuracy at the 1% level or better.
- A calibration signal that should work for all receivers at all wavelengths
- The calibration signal is sufficiently strong, but it is only a small addition to the system temperature. Non-linearities in the SIS mixers and in the correlator bandpass calibration should be kept small. This should improve bandpass calibration, and the adjustment of the SIS mixer.

- This small signal is injected in the RF circuit, insuring good calibration of the entire system.
- The coupling mirror can be spun rapidly for continuous system gain calibration.
- The plan includes a scattering mirror, so that the lowest system temperatures are preserved.
- The receiver temperature is measured in our scheme, whereas, is is not determined in the chopper wheel method.

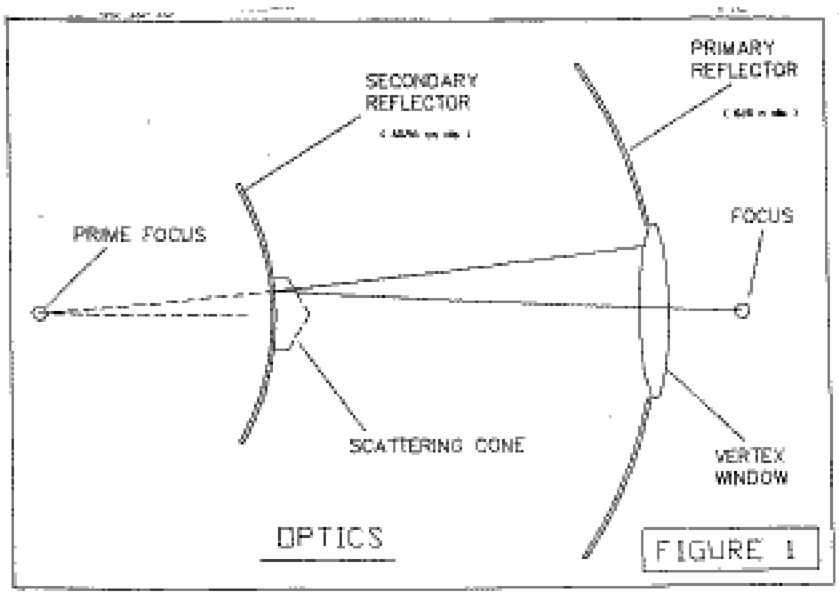
PRIMARY
REFLECTOR
SECONDARY
REFLECTOR
PRIME FOCUS
FOCUS
SCATTERING CONE
VERTEX
WINDOW
OPTICS
FIGURE 1

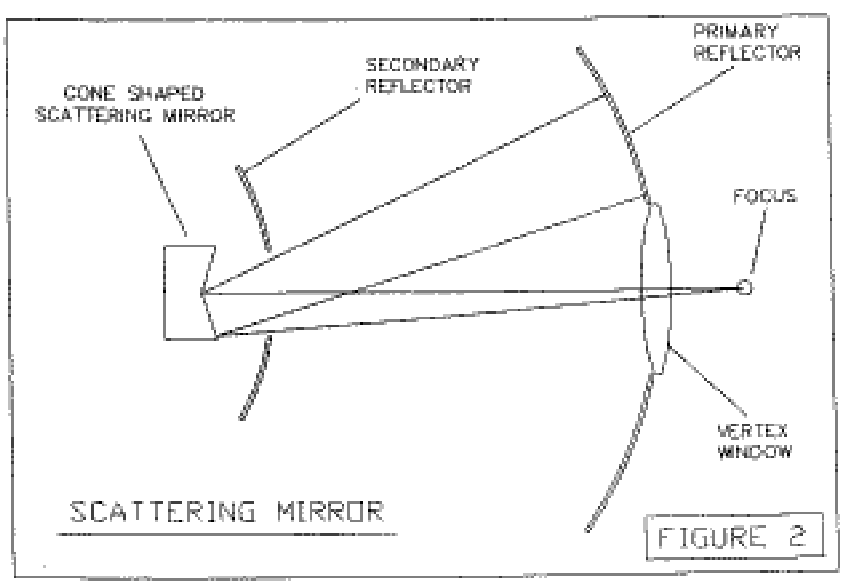
PRIMARY
REFLECTOR
SECONDARY
REFLECTOR
CONE SHAPED
SCATTERING MIRROR
FOCUS
VERTEX
WINDOW
SCATTERING MIRROR
FIGURE 2

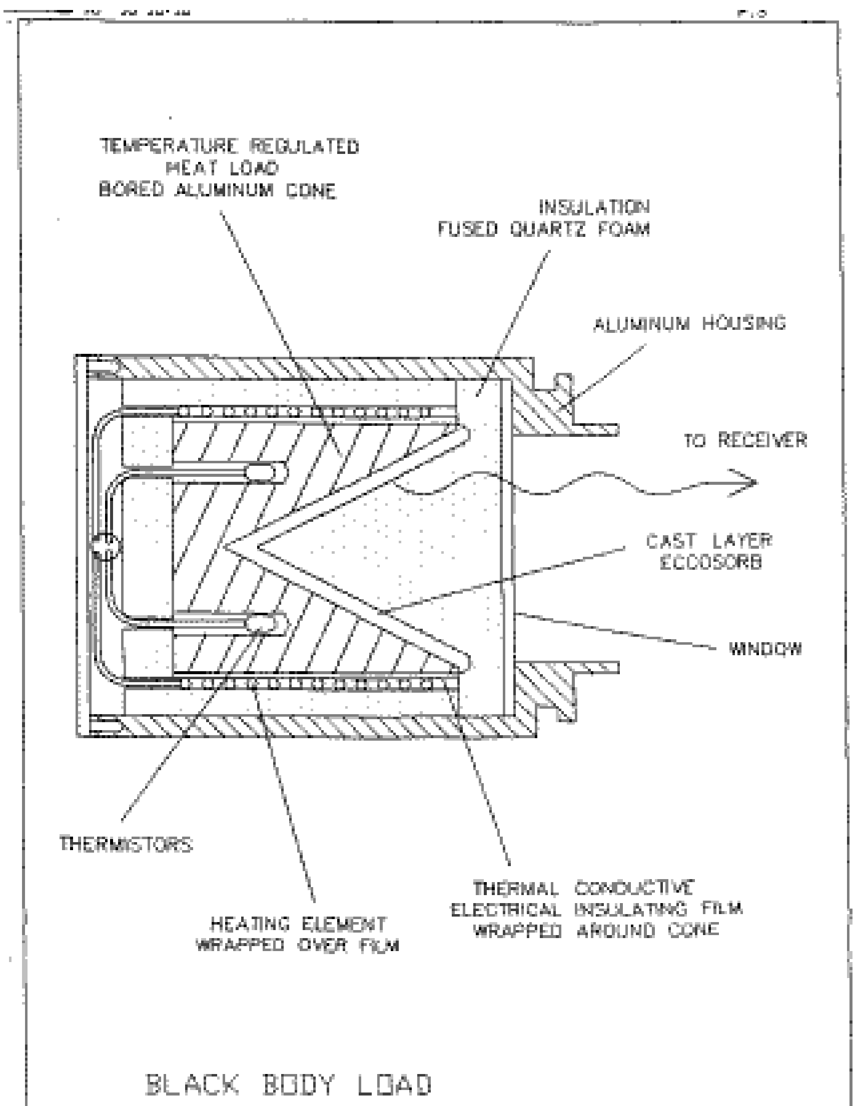
TEMPERATURE REGULATED
HEAT LOAD
BORED ALUMINUM CONE
INSULATION
FUSED QUARTZ FOAM
ALUMINUM HOUSING
TO RECEIVER
CAST LAYER
ECCOSORB
WINDOW
THERMISTORS
THERMAL CONDUCTIVE
ELECTRICAL INSULATING FILM
WRAPPED AROUND CONE
HEATING ELEMENT
WRAPPED OVER FILM
BLACK BODY LOAD

FIGURE 3

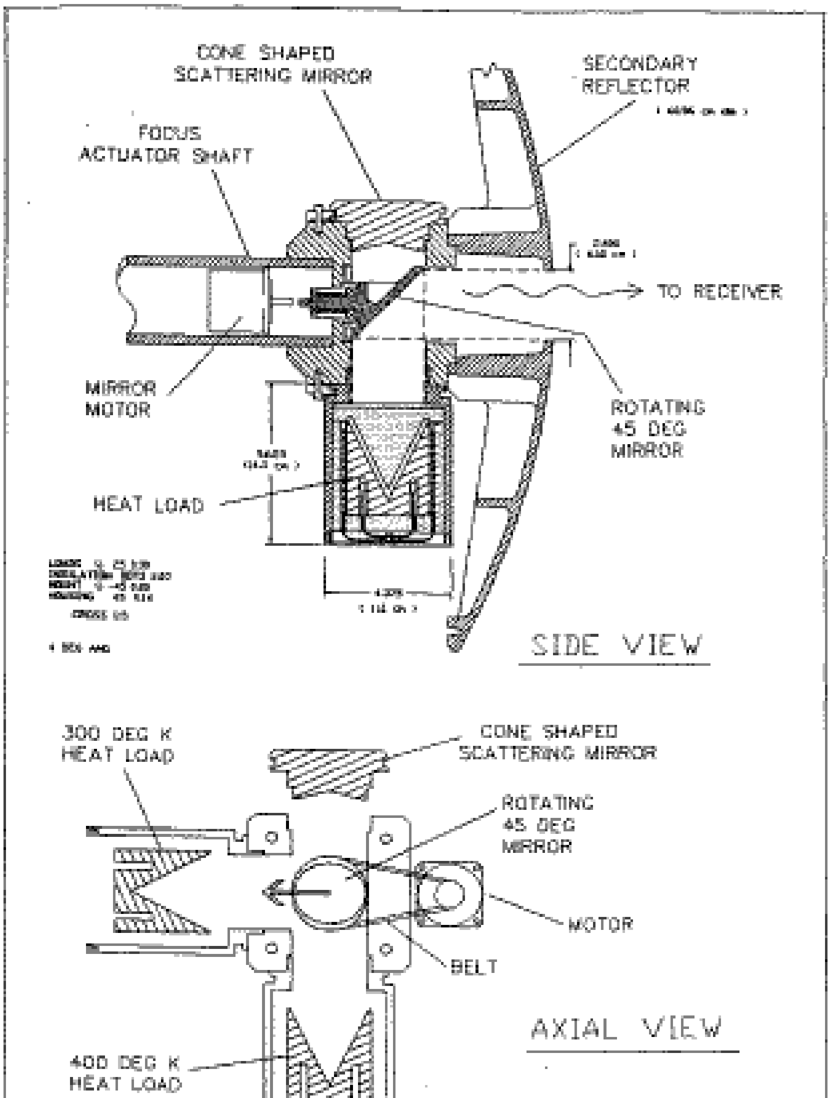
CONE SHAPED
SCATTERING MIRROR
SECONDARY
REFLECTOR
FOCUS
ACTUATOR SHAFT
TO RECEIVER
MIRROR
MOTOR
ROTATING
45 DEG
MIRROR
HEAT LOAD
SIDE VIEW
300 DEG K
HEAT LOAD
CONE SHAPED
SCATTERING MIRROR
ROTATING
45 DEG
MIRROR
MOTOR
BELT
AXIAL VIEW
400 DEG K
HEAT LOAD

FIGURE 4